



Paper

Cite this article: Pritchard HD, King EC, Goodger DJ, McCarthy M, Mayer C, Kayastha R (2020). Towards Bedmap Himalayas: development of an airborne ice-sounding radar for glacier thickness surveys in High-Mountain Asia. *Annals of Glaciology* 1–11. <https://doi.org/10.1017/aog.2020.29>

Received: 28 November 2019

Revised: 15 April 2020

Accepted: 27 April 2020

Key words:

Airborne electromagnetic soundings; ground-penetrating radar; ice thickness measurements

Author for correspondence:

H. D. Pritchard,

E-mail: hpri@bas.ac.uk

Towards Bedmap Himalayas: development of an airborne ice-sounding radar for glacier thickness surveys in High-Mountain Asia

H. D. Pritchard¹, E. C. King¹, D. J. Goodger¹, M. McCarthy^{1,2} , C. Mayer³ and R. Kayastha⁴

¹British Antarctic Survey, Cambridge, UK; ²Swiss Federal Institute for Snow, Forest and Landscape Research, WSL, Birmensdorf, Switzerland; ³Geodesy and Glaciology, Bavarian Academy of Sciences and Humanities, Munich, Germany and ⁴Department of Environmental Science and Engineering, Kathmandu University, Kathmandu, Nepal

Abstract

The thickness of glaciers in High-Mountain Asia (HMA) is critical in determining when the ice reserve will be lost as these glaciers thin but is remarkably poorly known because very few measurements have been made. Through a series of ground-based and airborne field tests, we have adapted a low-frequency ice-penetrating radar developed originally for Antarctic over-snow surveys, for deployment as a helicopter-borne system to increase the number of measurements. The manoeuvrability provided by helicopters and the ability of our system to detect glacier beds through thick, dirty, temperate ice makes it well suited to increase greatly the sample of measurements available for calibrating ice thickness models on the regional and global scale. The Bedmap Himalayas radar-survey system can reduce the uncertainty in present-day ice volumes and therefore in projections of when HMA's river catchments will lose this hydrological buffer against drought.

Introduction

There are ~90 000 glaciers in High-Mountain Asia (HMA) (Randolph Glacier Inventory Consortium, 2017) but very few have been surveyed for ice thickness. Only eight glaciers in the Hindu Kush-Himalayan arc are reported to have any thickness observations (GlaThiDa Consortium, 2019). Because ice thickness observations are used to calibrate glacier-thickness models there are therefore large uncertainties in estimated ice volumes on a regional scale (Farinotti and others, 2019), particularly where glacier thicknesses are substantially out of balance with contemporary climate (Farinotti and others, 2017). This uncertainty in volume translates directly into uncertainties in the lifespans of these glaciers as they shrink under the regime of negative mass balance that currently dominates (Brun and others, 2017) – a regime that is predicted to persist and intensify over future decades (IPCC, 2019), and will ultimately lead to a marked increase in drought stress when the ice reserve is lost (Pritchard, 2019). Ice-volume uncertainties can be reduced by better thickness-model calibration (e.g., Langhammer and others, 2019a), which requires a more extensive sample of measurements that are representative of the variety of topographic and climatic glacier settings in HMA.

The scarcity of existing data reflects the difficulty of surveying glaciers that are remote, at high altitude, contain temperate ice, have rough, wet and debris-covered surfaces in their lower reaches, and are steep, crevassed and highly avalanche-prone higher up. Airborne radar surveys over the ice sheets, using modified fixed-wing aircraft, are well established (e.g., Swithinbank, 1969; Schroeder and others, 2020), but most such systems operate at relatively high frequencies (≥ 60 MHz) suited to penetrating cold, clean ice sheets. On the ablation areas of mountain glaciers, where much of the ice volume is stored, a combination of greater surface reflectivity and higher signal attenuation in wet, debris-covered ice means that lower frequencies are preferable (Nobes and others, 1994; Gades and others, 2000). Fixed-wing aircraft have been used to tow low-frequency (1–2.5 MHz) dipole radars to sound through up to 1250 m of temperate ice in Alaska and Patagonia (Conway and others, 2009; Zamora and others, 2009; Rignot and others, 2013), but the reduced manoeuvrability of such aircraft at high altitude makes them unsuited to surveys in HMA, where high mountain walls surround narrow glacier tongues lying largely above 4000 m altitude.

Helicopters are typically used in such settings, and helicopter-borne radar systems have been deployed with some success at relatively low frequencies over temperate alpine glaciers (Kennett and others, 1993; Rutishauser and others, 2016; Langhammer and others, 2019b). A comparison of three systems found that a 30 MHz pulsed broadband radar was better at detecting the bed than higher-frequency (55–150 and 70 MHz) stepped and pulsed-broadband systems on temperate, largely debris-free alpine glaciers with thickness averaging 108 m (Rutishauser and others, 2016). The success rate for the 30 MHz system ranged from 47 to 69% of profile distance, depending on ice thickness (Rutishauser and others, 2016), and in places, it detected the bed through more than 700 m of temperate ice (Blindow and others, 2012; Rutishauser and others, 2016). There is evidence that antenna orientation parallel to ice flow yields a somewhat stronger bed signal in 25 MHz data in a low-clutter environment over largely debris-free ice (Langhammer and others, 2019b). However, these helicopter

© The Author(s), 2020. Published by Cambridge University Press. This is an Open Access article, distributed under the terms of the Creative Commons Attribution licence (<http://creativecommons.org/licenses/by/4.0/>), which permits unrestricted re-use, distribution, and reproduction in any medium, provided the original work is properly cited.

[cambridge.org/aog](https://www.cambridge.org/aog)

systems have not yet been tested on thick, high-altitude, debris-covered temperate mountain glaciers. The goal of this study was to develop a helicopter radar system able to operate at frequencies low enough to sound through the thickest HMA glaciers (>400 m), thus making it capable of filling the major ice-thickness data gaps in these ranges.

Specifically, we:

- (1) Carried out a number of ground-based field tests to determine bed detectability using different operating frequencies, stacking parameters and antenna orientations parallel and perpendicular to glacier flow.
- (2) Used the results of these tests in conjunction with aerodynamic modelling to inform the design of a helicopter-borne radar system.
- (3) Carried out survey flight tests of this new airborne system.

Ground-based field tests

Helicopter surveying imposes practical constraints on the shape, maximum size and weight of the survey instrument and the minimum speed of travel over the target glaciers, all of which influence the instrument design. Maximum length is particularly relevant to this study as it governs the minimum frequency that we can achieve with a dipole radar, where frequency is a first-order control on the penetration depth of radar signals into ice. Minimum flying speed is also relevant because it determines the minimum horizontal distance that is covered by each averaged 'stack' of radar traces along the survey track, for a given transmitter pulse-repetition frequency and digitisation rate, and this is a key control on the signal-to-noise ratio (SNR). In addition, the design of the survey pattern, particularly the profile direction relative to the valley axis and proximity to valley walls, is likely to influence the extent of radar clutter in the radargrams, which may hinder bed detection and affects the flying time, and therefore cost, of the survey.

The aim of our ground-based field tests was therefore to assess the sensitivity of the key criterion – bed detectability – to the choice of frequency, stacking and survey pattern, in challenging real-world conditions. The particular challenges for bed detection that we envisaged, in addition to potentially several hundred metres of ice, were the possible effects of the layer of rock debris of unknown thickness that mantles the surfaces of many Himalayan glaciers, and the wetness of the glacier surface in the target ablation areas during the melt season. We chose our test locations and timing to try to maximise the challenge to our system, and we assessed the character of the glacier surface at our study sites.

The main questions were broadly:

- (i) What minimum length (maximum frequency) of dipole antennas do we need in order to detect with confidence the bed of the test glaciers?
- (ii) For frequencies that penetrate to the bed, how many traces need to be stacked to maintain a detectable bed signal above the system noise? What does this mean for the minimum spacing of stacks during an airborne survey?
- (iii) How large are the clutter signals relative to the bed signal, and how do they vary with frequency and survey pattern?

Glacier and debris characteristics

We carried out a combination of survey profiles and static field tests on the ground during consecutive spring melt seasons on the debris-covered ablation-area tongues of Lirung, Langtang and Ngozumpa glaciers in Nepal (Fig. 1), chosen to be particularly challenging targets for radar sounding due to a combination of thick and at least partially temperate ice, and a surface debris

cover. Our tests coincided with a diurnal freeze-thaw cycle with a wet ice surface during the day (overlain by a wet snow layer on Lirung and Langtang glaciers), and we observed surface ponding of water at each site. Given the survey locations in the ablation areas of these glaciers, which have extensive ponding and englacial drainage networks (e.g., Gulley and Benn, 2007), we assume the ice to be temperate for much of its depth (Miles and others, 2018). Our sites have a near-continuous debris cover, and we sampled the debris thickness using pit measurements and relatively high-frequency ground-penetrating radar (GPR) profiles (McCarthy and others, 2017; Nicholson and others, 2018).

Debris-thickness pit measurements and surface observations at our sites in Nepal showed clasts ranging from silt to large boulders several metres in diameter, but predominantly gravels with air-filled voids near the surface grading to gravel with wet sand- and silt-filled voids in the centimetres to decimetres above the ice interface (McCarthy and others, 2017; Nicholson and others, 2018). The pit and GPR measurements showed debris thickness to be locally variable, ranging from 0.11 (range 0.01–0.34 m) to 2.3 ± 0.39 m and typically ~ 1 m on Lirung Glacier, and from 0.18 ± 0.14 to 7.3 ± 0.83 m, typically ~ 2 m on Ngozumpa. These debris characteristics are similar to and at least as thick as those found elsewhere, (e.g., Foster and others, 2012), and are at least an order of magnitude smaller than the radar wavelengths tested here. These findings reassure us that our sites are reasonably representative of challenging debris-covered ablation areas, and that the debris layer is thin enough and sufficiently well drained through much of its depth that it is unlikely to modify significantly the dielectric or scattering properties of the glacier/air interface as sensed by our low-frequency radar system. Such debris layers are therefore unlikely to be a major impediment to detecting the glacier bed.

Radar profiles

Dipole radars are effective transmitters and benefit from a linear antenna design whose simplicity makes them relatively easy to incorporate into a robust system for dragging over glacier surfaces (e.g., Evans, 1963). Design of a dipole radar for airborne deployment requires a compromise in antenna length that gives a centre frequency low enough to achieve bed detection in most expected conditions while still being short enough to allow portability of the system in the field. Our first goal was therefore to test several frequencies for bed detection in representative Himalayan glacial settings.

We surveyed for ice thickness on foot along a series of long- and cross-profiles (parallel and perpendicular to glacier flow, respectively) on our three test glaciers, primarily using the British Antarctic Survey DELORES dipole radar system. This is a mono-pulse radar capable of operating between 1 and 20 MHz, with a Kentech pulse transmitter that produces ± 2000 V pulses at a repetition rate of 1 kHz (King and others, 2008; Hindmarsh and others, 2011; King, 2011). It uses resistively loaded antennas that can be physically swapped to give a different centre frequency depending on antenna length. We used 40 and 20 m long dipoles for repeated profiles, giving centre frequencies of 3.5 and 7 MHz, respectively (Table 1), with received data converted from analogue signals with a 12-bit Picoscope digitiser.

We surveyed nine profiles over the lower tongues of Lirung and Langtang glaciers in March 2015, and eight profiles on Ngozumpa Glacier in April 2016, with sampling at 5 m intervals by stop-go surveys (Fig. 1). A stop-go approach rather than continuous surveys allowed us to control receiver/transmitter separation over rough ground. For most profiles, the transmitting and receiving antennas were arrayed line-astern with 30 to 50 m

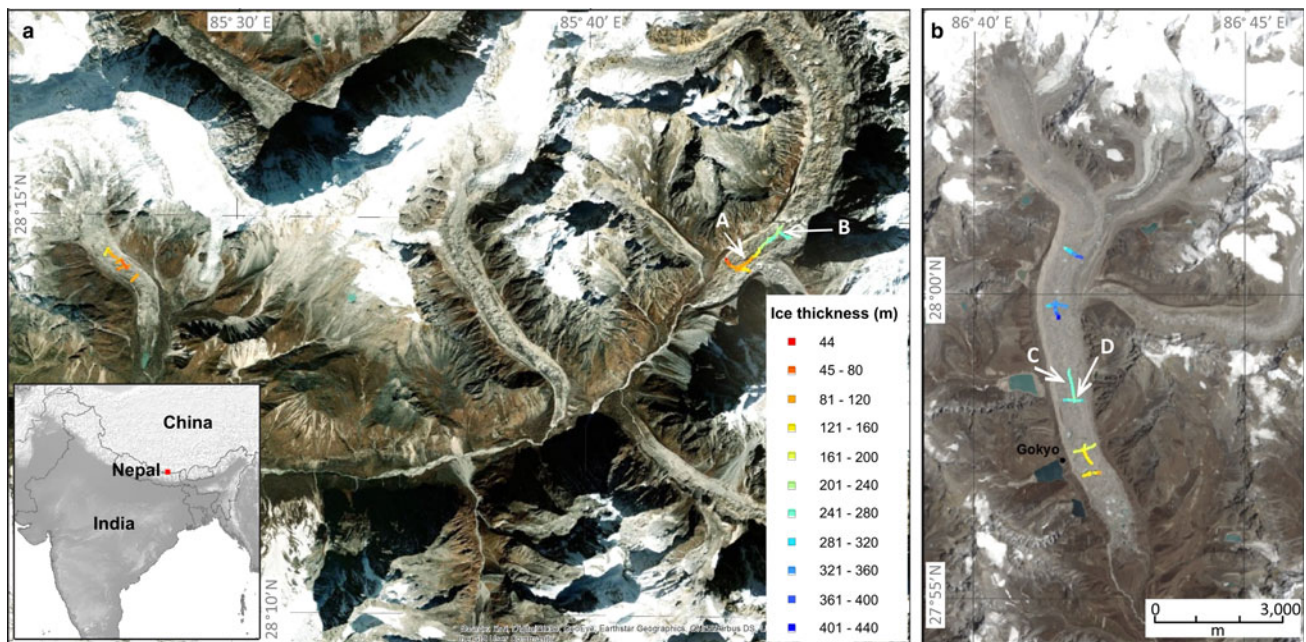


Fig. 1. Glacier ice thickness profiling results from glaciers (a) Lirung (left) and Langtang (right), and (b) Ngozumpa. Location of intersecting profiles discussed later are shown by white arrows. Image source: ESRI (GeoEye, DigitalGlobe).

Table 1. Radar characteristics

Centre frequency (MHz)	Dipole length (m)	Nominal wavelength in air (m)	Nominal wavelength in ice (m)	Nominal vertical resolution in ice (m)	Length of bed couplet (m) in Figure 4.	Optimal vertical resolution (m)	Practical vertical precision (m)	Fresnel zone radius at 280 m (m)
3.5	40	86	53	13	18	1	5	76
7	20	43	27	7	7	1	2	54
14	10	21	13	3	6	1	1	38

Nominal vertical resolution is the quarter-wavelength typically used to estimate the minimum resolvable separation of two similar reflectors (e.g., Reynolds, 1997). Optimal vertical resolution refers to the resolvable range to a single discrete, prominent reflector in an otherwise homogeneous medium (e.g., a smooth glacier bed below clean ice in a clutter-free environment) (King, 2020). Practical vertical precision refers to the distance observed in these data over which the bed couplet rises from the first break to the first peak (approximately one-quarter of the couplet length). This falls between the optimal and nominal resolutions and is a conservative estimate of the vertical distance over which the bed first break can be picked with confidence in these data. The Fresnel zone radius is calculated at 280 m because this is approximately the ice thickness of Langtang Glacier, and is indicative of the radar footprint size at the bed.

tip-to-tip antenna separation (a configuration familiar from Antarctic over-snow surveys), and each sample was taken as the stacked average of 4000 radar pulses. For two profiles on Ngozumpa Glacier, we experimented with a different system (Lambrecht and others, 2014) with antennas aligned in parallel at a 3 m lateral separation. Given the slower pulse-repetition frequency and digitiser speed of this system, each sample was taken as the stacked average of eight shots.

The separation of dipole antennas and their relative positions affects the system geometry. Relative to the antenna-parallel configuration, the line-astern separation primarily used here increased the path length through ice by typically 6 m (typically ~1% of the two-way travel distance) and increased the reflection angle at the bed (the separation between incoming and reflected signals) by typically 16°. These are, however, modest changes compared to those introduced by the variability in glacier thickness and antenna orientation along our undulating survey profiles, given the roughness of the surface. The more significant difference between these configurations is practical. Line-astern antennas are well suited to towed surveys over relatively smooth glacier surfaces (on foot or by vehicle), while over rough surfaces it is considerably easier for transmitter and receiver operators on foot to communicate and maintain a constant antenna separation using the parallel configuration. The disadvantage in parallel configuration is that the receiver is exposed to high peak power pulses from the adjacent transmitter, generally precluding the use of

amplifiers in the receiver. The parallel configuration is considerably shorter than line-astern, however, and therefore more likely to be suitable for an airborne system, hence we tested the practical application of both approaches in these tests.

Sample location was determined using post-processed differential GPS data. We processed radar data in ReflexW software using combinations of time-dependent divergence compensation, de-wowing (over a 300 ns moving window) and a band-pass frequency filter to aid manual detection of the glacier bed, and we corrected the resulting ice thicknesses for surface topography and system geometry. The band-pass filter lower cut-off, lower plateau, upper plateau and upper cut-off were 1, 2, 10 and 20 MHz for the 3.5 MHz profiles and 2, 4, 15 and 30 MHz for the 7 MHz profiles. We used a radar velocity in ice of 0.168 m ns^{-1} to convert two-way-travel times to ice thicknesses. Velocity depends somewhat on depth-averaged water content, however, which is unknown. Velocities of 0.165 and 0.172 m ns^{-1} have, for example, been ascribed to temperate and cold ice, respectively, above and below the equilibrium line of an alpine glacier (Macheret and others, 1993).

Radar profiles at 3.5 and 7 MHz produced radargrams with prominent linear or quasi-linear signals at various return times, and among these returns we identified the bed manually from its consistently linear nature throughout, and the agreement in depth and relative signal strength between long- and cross-profiles (e.g., Figs 2 and 3). Long-profiles from Langtang Glacier (Fig. 2)

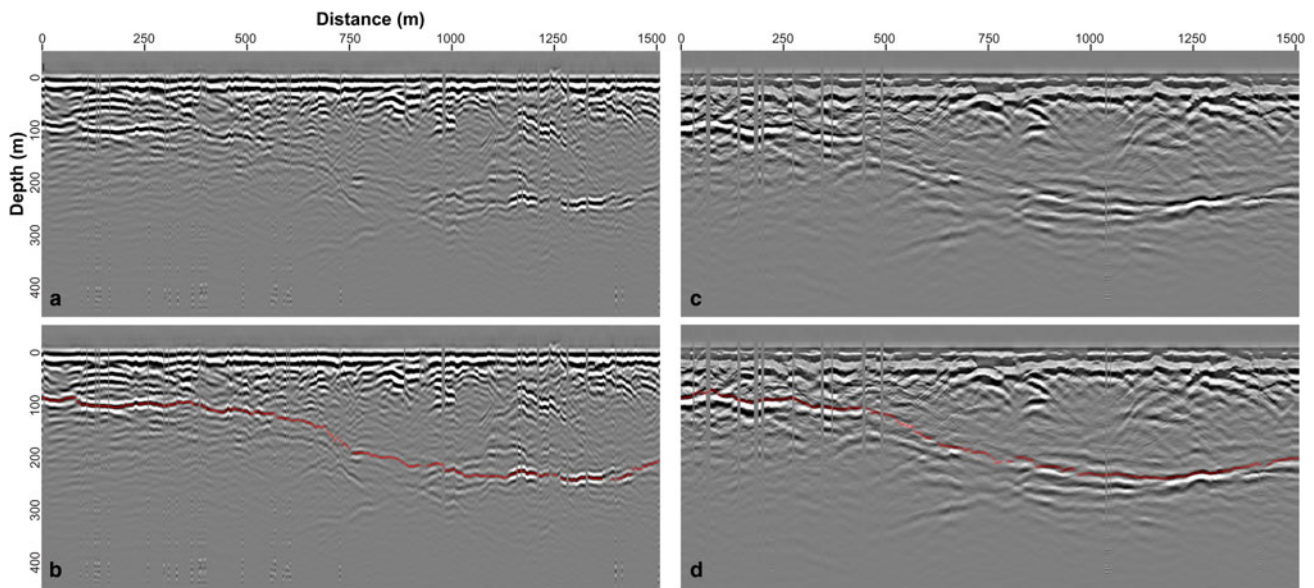


Fig. 2. Long-profiles with de-wow, divergence compensation and band-pass filtering from the lower Langtang Glacier (Label A in Fig. 1) at 7 MHz (a) and with bed pick (b), and 3.5 MHz (c) and with bed pick (d).

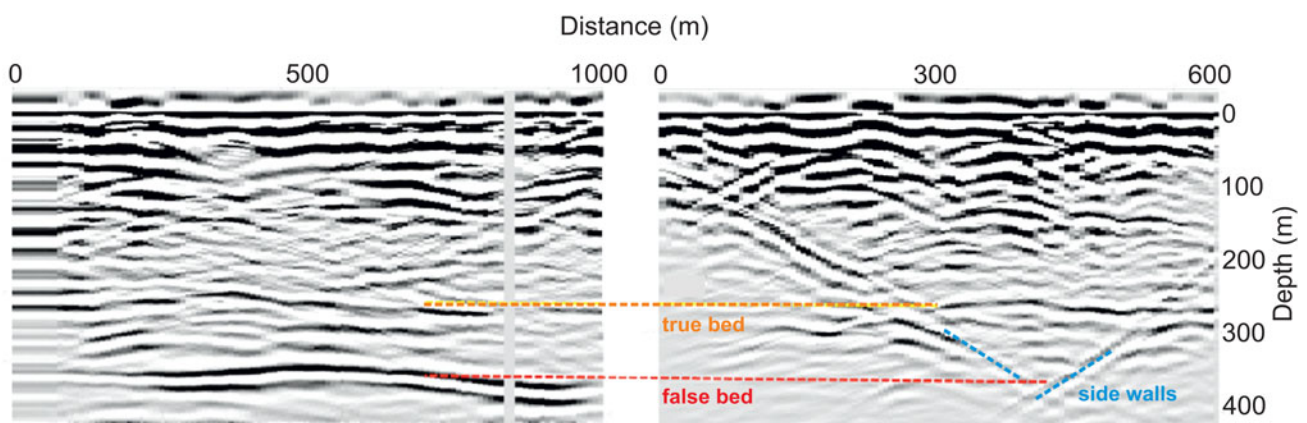


Fig. 3. (a) Long-profile (Label C in Fig. 1), and (b) intersecting cross-profile (Label D in Fig. 1) from Ngozumpa Glacier, at 3.5 MHz. The red dashed line indicates a prominent 'false bed', the yellow/orange line, the true bed. The blue dashed lines highlight the trend of the dipping reflectors from the valley walls to the east and west of the glacier.

demonstrate the detectability of the bed and the potential for higher horizontal resolution in the bed return at the higher frequency (comparing Figs 2b and d), as expected from the smaller Fresnel zone at higher frequencies (Table 1). They also highlight the ambiguity that arises in picking the bed return due to the presence of other nonbed signals.

We class these nonbed signals as clutter of unknown surface or englacial origin and note that this is often of similar strength to the bed signal or stronger, and present at similar return times. This leads to the potential for systematic bed-misidentification particularly in radar long-profiles of valley glaciers, where the range to the lateral moraines or valley walls (potential sources of additional reflections at similar return times) may be relatively constant. A prominent, linear, bed-like reflection in a long-profile from Ngozumpa Glacier (Fig. 3a), for example, is absent in a crossing profile (Fig. 3b), which shows linear, diagonally dipping returns from both valley sides, indicating that these are the source of the bed-like reflection. The true, shallower bed reflection is apparent in both profiles and is weaker, which we attribute to the greater signal attenuation through temperate ice than air.

Multiple blank traces and several with misaligned start times are apparent (e.g., in the first 600 m of Fig. 2c). This resulted from mis-triggering of the radar receiver from the transmitted airwave, a problem that was common when surveying on the undulating glacier surface with the transmit dipole trailing the receive dipole (by ~ 50 m tip-to-tip). Occasional loss of receiver-transmitter line-of-sight intervisibility caused unpredictable distortion of the airwave in some locations, which is difficult to accommodate when setting airwave-triggering parameters during ground surveys. For thickness mapping we corrected mistimed traces in post-processing. Our survey profiles reveal ice thicknesses ranging from ~ 40 to 440 m, with the deepest ice present in the central trunk of Ngozumpa, Nepal's largest glacier (Fig. 1).

Static tests

Having established the ice thickness along our survey profiles, we also carried out static tests with and without receiver amplification at three frequencies (3.5, 7 and 14 MHz) in relatively flat areas of the glacier surface, to quantify the relationship between frequency and bed SNR and signal-to-clutter ratios (SCR). We defined the

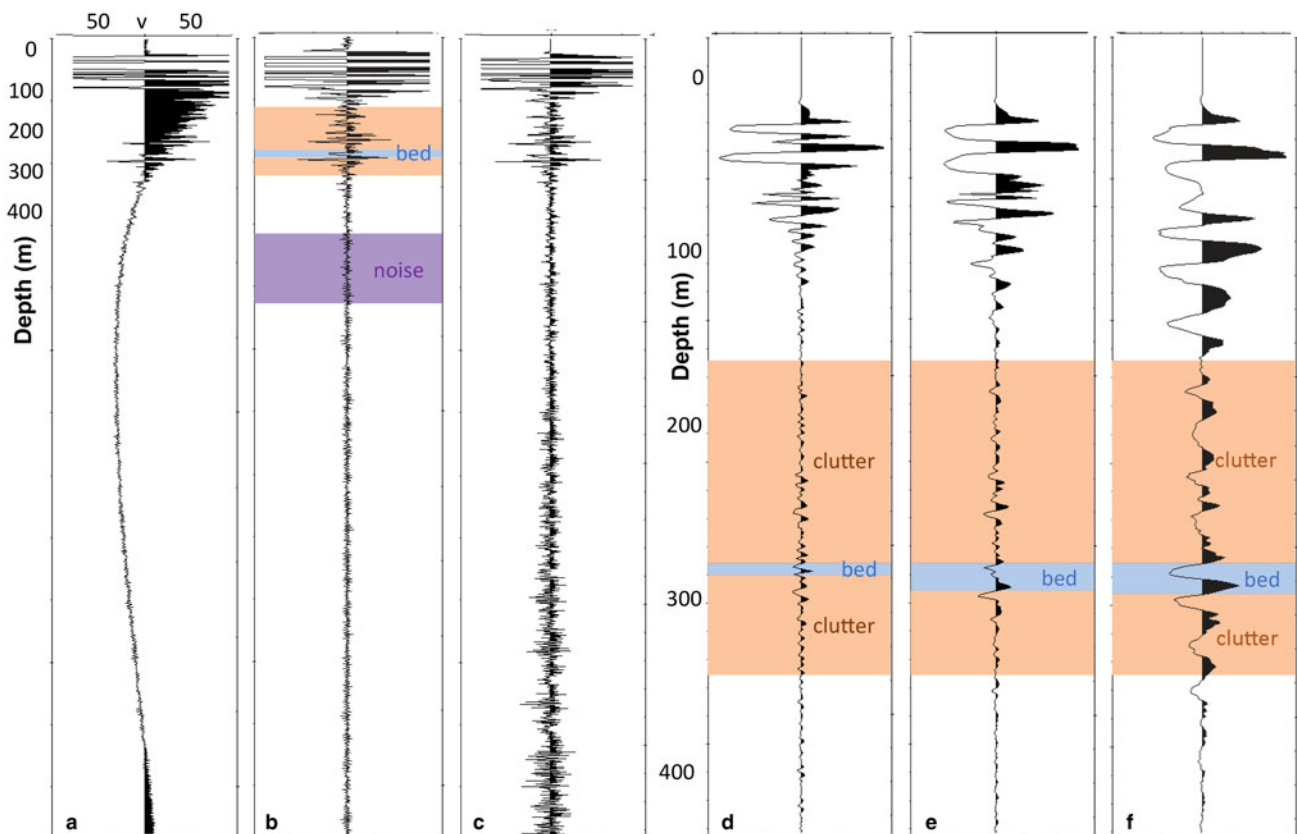


Fig. 4. Radar traces collected at a point on Langtang Glacier (intersection of profiles A and B in Figs 1 and 6), showing (a) a 7 MHz, amplified 1000-stack raw trace, (b) the same trace after processing for de-wow and (c) de-wow plus divergence-compensation, with the windows used to quantify the bed-signal SNR and SCR. (d) shows in detail the de-wow and divergence-compensated traces at 14 MHz, (e) 7 MHz, and (f) 3.5 MHz. The depth scale is corrected for the radar geometry and ice thickness is approximately 286 m.

bed signal as the mean absolute voltage of the bed-return wave couplet, clutter as the mean absolute voltage of nonbed signals in the range from 1500 ns before to 600 ns after the bed return (after de-wow processing with a 300 ns window), and noise as the mean absolute voltage of the far-field recorded signal (covering a period of 2000 ns starting at 2000 ns after the end of the bed return), after de-wow and ReflexW's time-dependent divergence-compensation processing (Fig. 4). We chose the signal, noise and clutter time windows through manual interpretation of the traces. The window that defines clutter brackets the known bed depth, beginning after the prominent declining trend of signal amplitude in the early part of the record and ending as the signal drops close to the apparent noise floor at the higher frequencies tested (Fig. 4). The noise window begins after the onset of the noise floor at all three frequencies. These static tests over a bed of depth known from the profiling surveys allowed us to compare the bed SNR and SCR at three frequencies (Table 1, locations of intersections in Fig. 1).

We found that the detectability of the bed signal relative to both noise and clutter is primarily dependent on frequency, with a weaker dependency on stacking (Fig. 5). Clutter is the dominant constraint on bed detectability, with SCR not exceeding 3 while the SNR exceeded 70 in amplified data and 9 in unamplified data. Stacking helps to increase the SNR by averaging randomly varying noise but has little effect in boosting the SCR because the clutter signals, like the bed signal, are consistent through time. Note that because noise suppression through stacking is ultimately limited by the precision (bit-depth) of the digitiser, a higher SNR could be achieved by changing from the 12-bit Picoscope digitiser to a 14-bit system, which we subsequently did (see 'Antenna configuration').

The higher SNR of the bed at lower frequencies is expected given that attenuation increases in proportion to the square of the frequency in ice and fresh water (e.g., Page and Ramseier, 1975; Davis and Annan, 1989), hence at lower frequencies less signal is lost, while in contrast, system noise is frequency-independent. There is also some weaker frequency-dependence apparent in the SCR (Fig. 5, dashed lines, right axis), but it is less clear why the clutter and bed signal-strength should respond differently with frequency.

This could arise if the bed signal is preferentially weakened at higher frequencies through attenuation as described above, while in contrast, the clutter comes primarily from the glacier surface, travels largely unattenuated through air and therefore changes little with frequency. It could alternatively arise if the dominant clutter reflectors are effectively point scatterers of similar size to the shorter wavelengths tested (on the scale of metres), and substantially smaller than the longest wavelengths (close to 100 m) (Table 1). For a flat-plate scatterer of a given physical area and dielectric properties, the radar cross section (i.e., backscatter strength) is inversely proportional to the wavelength squared (Bole and others, 2014), hence clutter would be weaker at lower frequencies for such relatively small scatterers. Likely contributors to clutter that are within the ranges observed are the hummocky, wet and debris-covered glacier surface, as well as debris- and water-filled crevasses, wet ice cliffs and water-filled englacial channels and ponds. In addition, the lateral moraines should contribute airwave reflections with relatively little attenuation around the time of the returning bed signal, given the faster signal propagation rate and lower attenuation in air (Fig. 6). Further static tests in a variety of settings are needed to understand better the relationship between frequency and clutter.

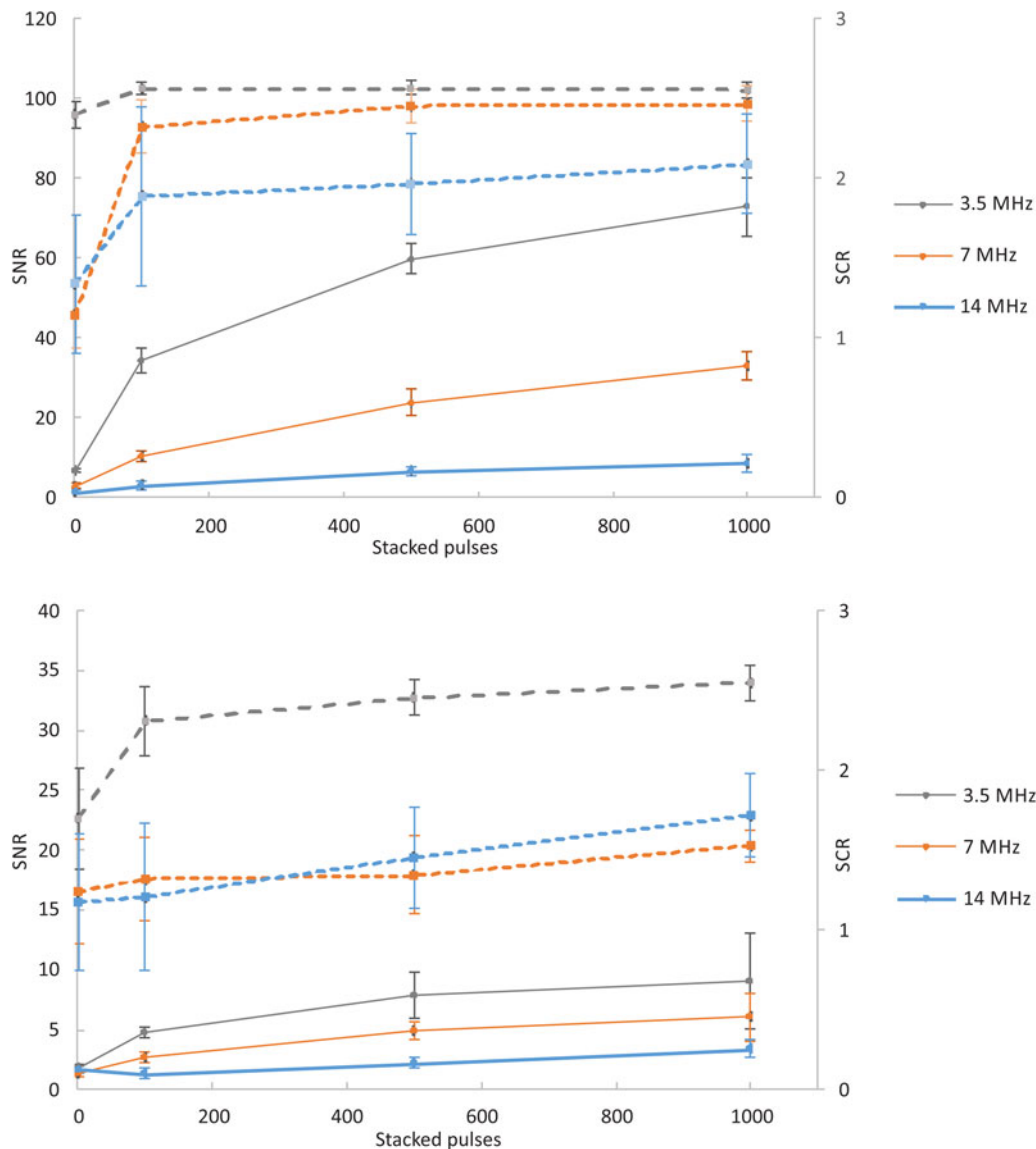


Fig. 5. Bed SNR (solid lines, left axis) and bed SCR (dashed lines, right axis) varying with stacking for the three frequencies tested for (a) amplified and (b) unamplified data. Error bars show ± 1 Std dev. of the ratios measured over 11 repeated stacks for each configuration.

Conclusion of the ground-based tests

The tests conducted in this study show that in this Himalayan context, glacier beds are increasingly detectable with respect to both noise and clutter as frequency decreases from 14, to 7 and 3.5 MHz. With sufficient stacking, the bed signal in our static tests was at least several times greater than noise at each of these frequencies through a typical debris layer of order 1 m thick, and through ~ 280 m of temperate ice in thawing conditions. Greater bed detectability at lower frequencies comes at the expense of horizontal and vertical resolution, which decrease from tens of metres to order 100 m in the horizontal and nominally from ~ 5 to ~ 20 m in the vertical at the lowest frequency, though we conservatively estimate that the practical vertical precision of the bed depth actually decreases from ~ 1 to ~ 5 m over these frequencies (Table 1).

Clutter made bed detection ambiguous in static datasets at each frequency (Fig. 4). Travelling profiles aided interpretation of the continuous, quasi-linear bed reflection as distinct from clutter that is typically less continuous along a profile, and at 3.5 and 7 MHz the bed was identifiable at all surveyed ice thicknesses, which exceeded 400 m. In data collected along central-glacier long-profiles

however, strong and continuous valley sidewall reflections were sometimes present at a similar time delay to the more-attenuated bed signal, and in such cases cross-profiles are invaluable in distinguishing between sidewall clutter and bed signals.

These tests imply that for an airborne dipole radar for ice-thickness surveys, a frequency of 7 MHz or lower (length of 20 m or longer, Table 1) and stacking of several hundred are preferable, and that survey flightpaths should include multiple glacier cross-profiles in addition to a central long-profile. With this stacking, a 1 kHz transmitter and a flight speed of 50 km h^{-1} , for example, a horizontal sampling interval of ~ 10 m is achievable. This is substantially smaller than the Fresnel zone radius (Table 1), is finer than the resolution needed for glacier-volume calculations, and confirms that stacking is not a limiting factor for airborne deployment of our radar system at reasonable flight speeds.

Development of the helicopter radar system

Antenna configuration

Based on the findings of the ground tests, we developed and tested an antenna configuration to maximise length while seeking a

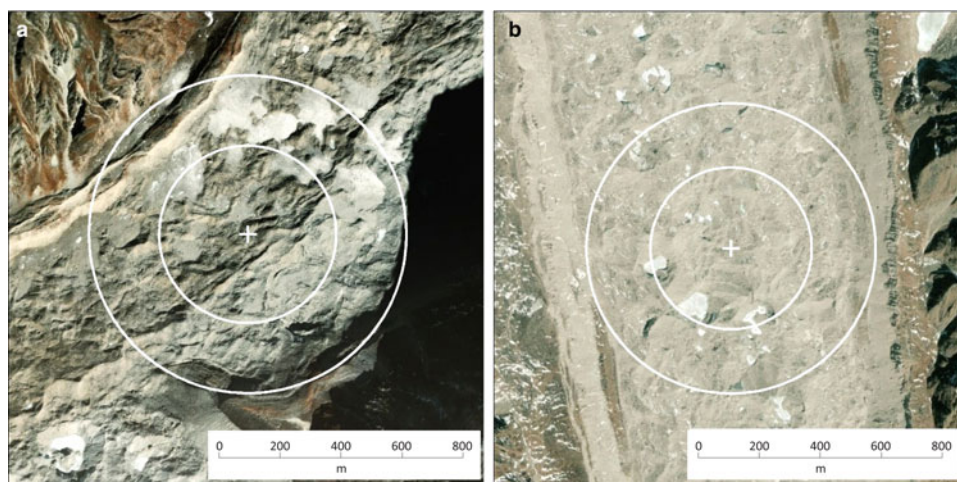


Fig. 6. (a) Langtang Glacier and (b) Ngozumpa Glacier radar static-test sites (locations at the AB and CD intersections in Fig. 1). White circles show horizontal ranges that are equivalent to the bed depth for radar propagation speeds through ice (inner circle) and through air (outer circle). Surface features corresponding approximately with the outer circle could provide clutter with a similar time delay as the bed signal. Image source: ESRI (GeoEye, DigitalGlobe).

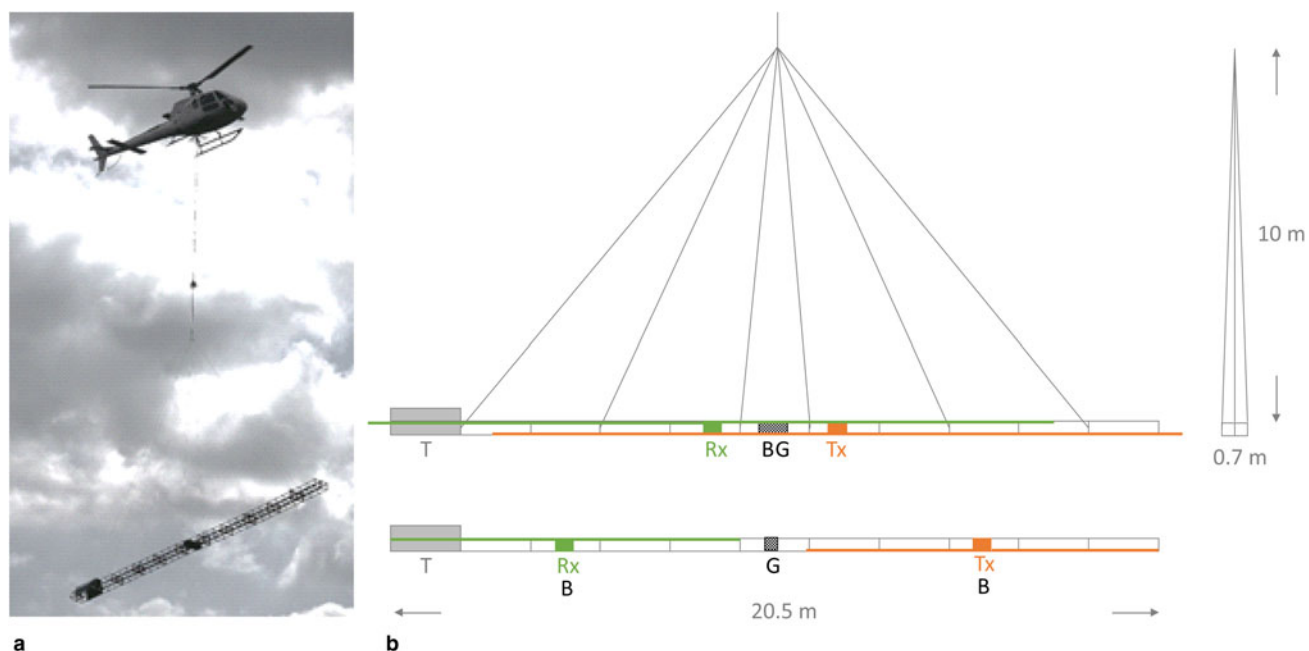


Fig. 7. (a) Full-scale airframe prototype. (b) Schematic of radar components, shown configured for 8 MHz (top) and 16 MHz (bottom). Rx and Tx refer to the receiver and transmitter units and antennas, T to the tail, B to battery and G to GPS.

compromise with the practical constraints of an airborne system. At ~ 100 m long, the typical line-astern dipole configuration for ground surveys at the lower end of the frequency range considered is not feasible for helicopter deployment. We therefore considered switching between transmit and receive on a single dipole, but the high instantaneous pulse power, wide bandwidth and very low duty cycle of our transmitter (Kentech Instruments Ltd. GPR Pulser J10) made this impractical. Our ground tests (section 'Radar profiles') showed, however, that a separate and overlapping matching pair of resistively-loaded receiver and transmitter dipoles in parallel could also be used, provided that the receiver digitiser is protected from pulse overload when the antennas are brought close together. Because our antennas are resistively loaded (with resistance increasing towards the tips), we were able to limit the peak received power to below the operational limits of the digitiser by staggering the parallel receiver and transmitter dipoles by 4.8 m (Fig. 7).

Deploying the antennas in parallel rather than line-astern reduces the system length by $\sim 70\%$, though the close proximity of transmitter and receiver preclude the incorporation of amplifiers in the receiver system. We were able to compensate for this by introducing a high-precision, 14-bit Teledyne SP Devices digitiser (rather than the 12-bit Picoscope used in the ground tests) to record two receiver data channels, one with a large dynamic range of ± 5 V covering a wide range of returning signals and the other covering ± 1 V to give enhanced sensitivity to weak signals. The high precision also makes stacking more effective at lowering the noise floor, and we used this high-sensitivity channel for bed detection when the SNR was low.

Airframe structure

Informed by the bed-detection field tests regarding antenna length, and constrained by the need for a light, robust, modular,

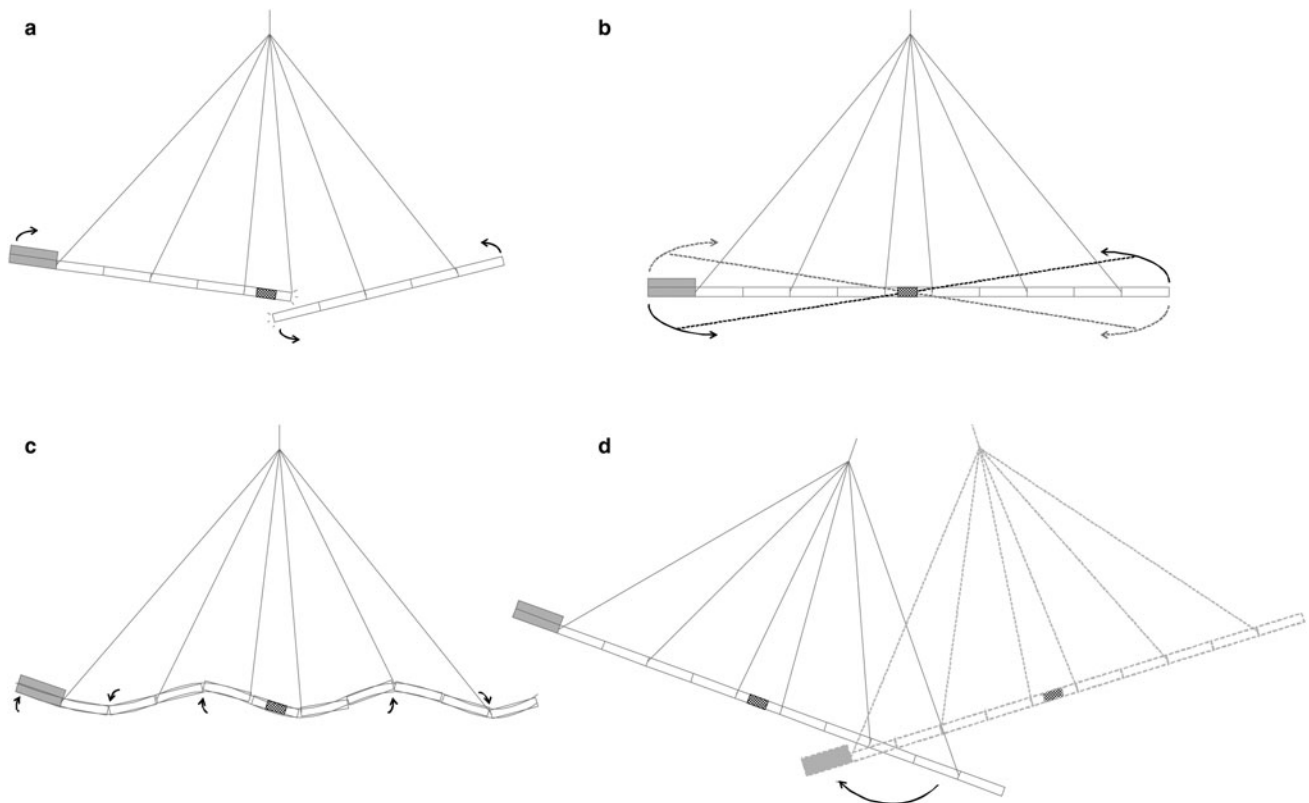


Fig. 8. (a) Buckling, and the oscillatory modes (b) weather-cocking, (c) flutter and (d) penduluming.

and electrically nonconductive frame design that can be operated safely by helicopter in high-mountain environments, we used modelling and prototyping to develop an elongated frame structure for suspension under an un-modified helicopter as a sling-load. We commissioned aerodynamic modelling (Graham and McRobie, 2017) to assess, for a frame-structure of up to 40 m long towed at airspeeds from 10 to 250 km h⁻¹, resilience to buckling and tendency to the oscillatory motions of fluttering, weather-cocking and penduluming that could cause structural fatigue and failure (Fig. 8).

Buckling forces are controlled by the angle between the guy-lines and the frame and the wind forces experienced by the structure, which depends on frame drag, frame attitude in flight and flying speed. Buckling calculations therefore informed decisions on frame length, rigidity, strength and weight (as a control on attitude), and on the height above the frame of the guy-line apex (yoke). The modelling identified potential weather-cocking and penduluming oscillatory motions but predicted both to be stable at all speeds tested, i.e., to decay with time rather than amplify. Their frequencies were predicted to differ (weather-cocking in most cases lower than penduluming) and although no mode-interactions were found to be unstable, such interactions are difficult to predict so we aimed for a design that kept these frequencies apart. Specifically, we aimed to maintain a relatively low weather-cocking frequency by providing sufficient resistance to yaw and by limiting the maximum flying speed, and a relatively high penduluming frequency by minimising the total suspended length, while maintaining a yoke height sufficient to prevent buckling. We also took into consideration test results showing that, due to drag effects, both oscillations decayed more rapidly as the number of guy-lines increased, and that flutter is reduced by increasing frame rigidity (Appendix).

For prototyping, we designed a modular system based on a set of box-frames constructed of polyester resin fibreglass tubes and glass-filled nylon couplings, with each frame 1.87 m × 0.35 m ×

0.35 m and weighing 7 kg. Twenty-two frames strapped in an 11 × 2 configuration gives a 20.5 m-long airframe that retains some flexibility and an acceptably light weight for field deployment, and the length can readily be extended by using additional single fibreglass poles at each end. We suspended the whole frame from a set of high-breaking-strain, low-stretch guy-lines that meet 10 m above at a central yoke, and latch to a standard helicopter load sling for survey flights. To resist yaw, we doubled the height of the tail section and wrapped it in waterproof fabric (Fig. 7). Symmetrically in this frame, we mounted the radar transmitter, receiver and battery in waterproof plastic cases, with antenna wires attached to the frame structure. The total system weight is ~230 kg with a 100 Ah lead-acid battery. With a parallel transmit-and-receive dipole configuration, our 20.5 m-long system can provide transmitted radar frequencies as low as 7 MHz.

We suspended our prototype from cranes to test for rigidity and structural integrity, and conducted airborne helicopter flight tests for aerodynamic performance and structural integrity in straight flight at various speeds, and in turns, climbs and descents.

Survey testing of the helicopter radar

Structural design

In 5 hours of helicopter flight tests in the UK and Svalbard between February and April 2018, our frame design performed well aerodynamically at intended survey speeds of ~30 knots (55 km h⁻¹) and up to the maximum-tested 50 knots (90 km h⁻¹), maintaining an attitude aligned with the flight direction and reliably returning to this attitude after short-radius (100 m) turns through 180°. The frame showed no tendency to oscillate or rotate in flight and remained under good control, allowing surveys to be conducted at helicopter flying heights of 75–90 m (250–300 feet) with a ground clearance for the radar of 50–65 m (165–

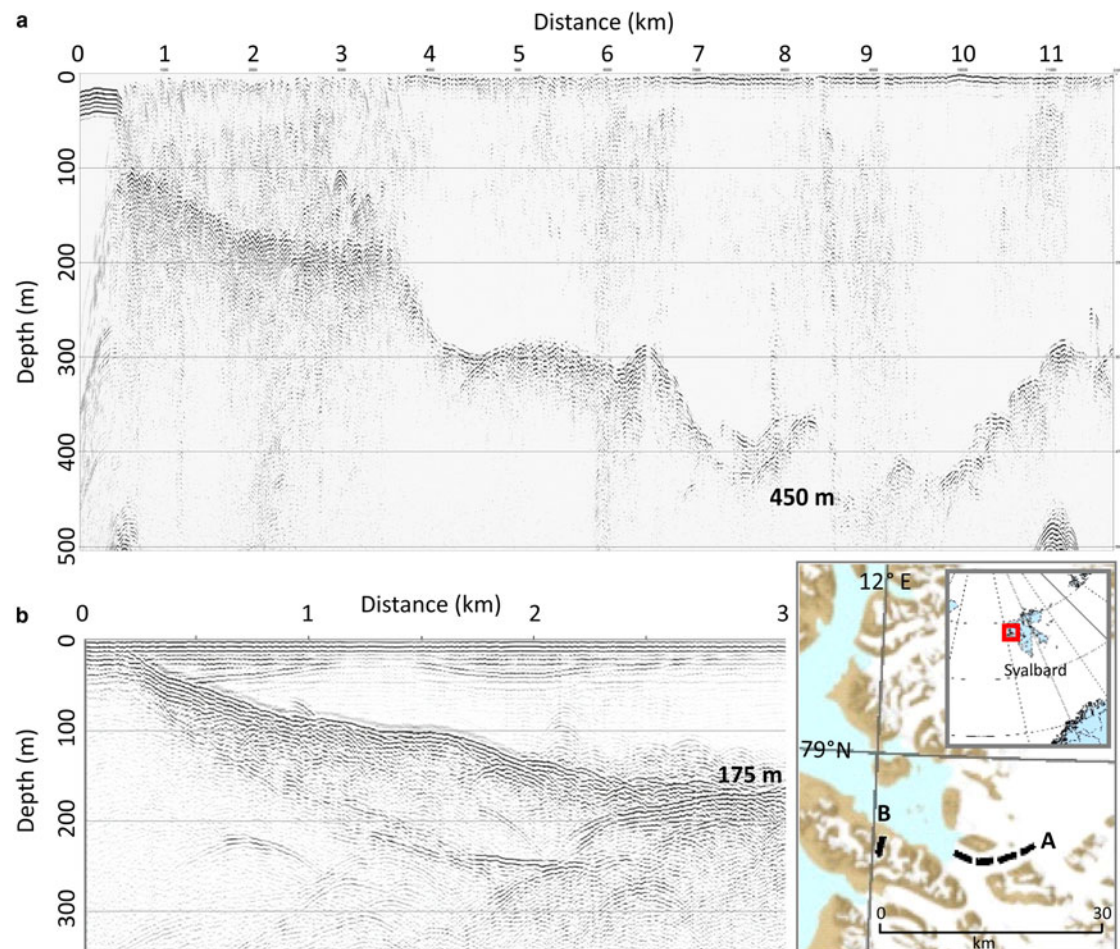


Fig. 9. Helicopter-surveyed longitudinal profiles over (a) the lower 13 km of Kronebreen, and (b) the lower 3 km of Midtre Lovenbreen, Svalbard. We calculated depths using a wave speed of 0.168 m ns^{-1} in ice. For the heavily crevassed Kronebreen, post-processing with a horizontal averaging filter and a manual gain curve suppressed surface-crevasse clutter by 19 dB. Map data: ESRI.

210 feet). Post-flight inspections showed no evidence of structural fatigue or damage.

Flight surveys

To test our full frame and radar system we flew three survey flights in Svalbard. The primary goal of these flights was to test our frame for aerodynamic issues experienced by the helicopter crew during prolonged flight operations, and to test for ease of shipping, construction and operational use, and for structural performance and robustness of the frame in cold field conditions. The secondary goal was to run our radar in-flight to test for electrical interference issues with the helicopter (both in terms of flight operations and radar data quality), and for robustness of our electrical system in survey use. The tertiary goal was to test radar-data acquisition and storage performance by surveying over our target glaciers using a simple radar configuration of known capability that we have used in previous polar surveys.

For simplicity, we configured the radar on our 20.5 m frame with separated (nonoverlapping) 8 m-long, line-astern transmit and receive antennas (giving a 16 MHz centre frequency), with the receiver unamplified and triggered from the airwave (Fig. 7). We flew this over the small, polythermal, land-terminating and largely un-crevassed Midtre Lovenbreen, Svalbard, where equivalent 16 MHz ground-survey data were previously collected by one of the authors (E. King) and so were available for validation if needed (not presented here). We also

flew two flights over thicker, heavily crevassed tidewater Kronebreen, where ground survey is not possible (Fig. 9).

These flight surveys demonstrated that our system design is aerodynamically and operationally robust and practical to deploy in field conditions, and did not suffer from interference with the helicopter. Even at a relatively high frequency (and relatively low stacking of 280), it detected the beds of the small, polythermal, land-terminating Midtre Lovenbreen and the large, heavily crevassed polythermal tidewater glacier Kronebreen throughout the survey profiles, through maximum encountered thicknesses of 175 and 450 m, respectively (Fig. 9).

In contrast to glacier conditions encountered in Nepal, the surfaces of these Svalbard glaciers were debris-free and frozen at the time of survey, however. Furthermore, physical decoupling of our airborne radar from the ground will introduce radar reflection losses from the glacier surface in addition to the attenuation losses present in our ground tests. Reflection is governed by the contrast in dielectric permittivity (ϵ) and therefore wave-speed between air ($\epsilon = 1$) and the glacier. Over melt ponds ($\epsilon = 86$ (Frolov and Macheret, 1999)) we expect reflection losses of $\sim 80\%$ (Wightman and others, 2003) but elsewhere we expect $\epsilon \approx 3$, dominated by the properties of ice and modified relatively little by the similar properties of the debris or wet snow cover ($\epsilon \approx 3$ to 5 (Frolov and Macheret, 1999; Grima and others, 2014)), that are anyway thin relative to the wavelength. At incidence normal to the surface, this implies reflection losses of $\sim 28\%$ (Wightman and others, 2003) (or up to 38% for $\epsilon = 5$ (Grima and others, 2014)). Additional spreading losses are also

introduced with an airborne system due to the 10–20% increase in range to the bed.

These factors decreasing the likely bed signal strength are partly offset by the smaller reflection angle ($\sim 0.004^\circ$) and fixed, horizontal antenna alignment of our airborne system relative to the line-astern ground surveys. The likely magnitude of these changes in signal strength relative to the SNR (unamplified) of 5–6 with achievable stacking rates (through ~ 300 m of ice at 7 MHz) that we observed in Nepal give us confidence that our airborne system is capable of detecting the beds of Himalayan glaciers.

Conclusions

Through a series of field and airborne tests we have developed a modular radar system that can be deployed by an unmodified helicopter to remote, high-mountain or polar settings where ground survey is impossible or impractically slow. Our helicopter system can operate at frequencies down to 7 MHz which in ground tests was sufficiently low to detect glacier beds with a high SNR at stacking rates that are achievable at typical flying speeds, in high-attenuation and high-clutter environments. These and our Arctic airborne tests indicate that our system is well suited to surveying heavily crevassed tidewater-glacier margins and heavily debris-mantled, large, temperate mountain glaciers, particularly when the survey combines long- and cross-profiles to reduce ambiguity from clutter.

The results of our ground-based surveys in Nepal demonstrate the value of such measurements. The mean surveyed thicknesses of the lower Langtang, Ngozumpa and Lirung glaciers are 155, 270 and 100 m, respectively (Fig. 1). Given the thinning rate of the Ngozumpa Glacier ablation zone of $0.64 \pm 0.18 \text{ m a}^{-1}$ from 2000 to 2015 (King and others, 2017), its lifespan can be projected as ~ 420 years. As the largest glacier in Nepal, this may be the last of Nepal's glaciers tongues to be lost. Applying the Khumbu-average thinning rate of $0.52 \pm 0.22 \text{ m a}^{-1}$ (King and others, 2017) to nearby Langtang and Lirung glacier tongues gives projected lifespans of ~ 300 and ~ 200 years, respectively. The point at which the glacier tongues are lost marks a major transition for the river catchments downstream as they lose their hydrological buffer against water shortages during summer droughts (e.g., Pritchard, 2019). As glaciers thin, the timing of this hydrological regime shift can only be determined if ice thickness is known, and with the Bedmap Himalayas airborne radar system, we now have the ability to provide these key observations.

Supplementary material. The supplementary material for this article can be found at <https://doi.org/10.1017/aog.2020.29>.

Acknowledgements and data availability. This project was supported by Natural Environment Research Council grants NE/L013258/1 and NE/R000107/1. Survey data are available from the Polar Data Centre of the British Antarctic Survey, reference NE/L013258/1.

References

- Blindow N, Salat C and Casassa G** (2012). Airborne GPR sounding of deep temperate glaciers – examples from the Northern Patagonian Icefield. *14th International Conference on Ground Penetrating Radar (GPR)*.
- Bole A, Wall A and Norris A** (2014) Chapter 3 – target detection. In Bole A, Wall A and Norris A (eds), *Radar and ARPA Manual*, 3rd Edn. Oxford: Butterworth-Heinemann, pp. 139–213.
- Brun F, Berthier E, Wagnon P, Kääb A and Treichler D** (2017) A spatially resolved estimate of High Mountain Asia glacier mass balances from 2000 to 2016. *Nature Geoscience* **10**, 668–673. doi: <https://doi.org/10.1038/ngeo2999>.
- Conway H and 5 others** (2009) A low-frequency ice-penetrating radar system adapted for use from an airplane: test results from Bering and Malaspina Glaciers, Alaska, USA. *Annals of Glaciology* **50**(51), 93–97.
- Davis JL and Annan AP** (1989) Ground-penetrating radar for high resolution mapping of soil and rock stratigraphy. *Geophysical Prospecting* **37**, 531–551. doi: [10.1111/j.1365-2478.1989.tb02221.x](https://doi.org/10.1111/j.1365-2478.1989.tb02221.x).
- Evans S** (1963) Radio techniques for the measurement of ice thickness. *Polar Record* **11**(73), 406–410.
- Farinotti D and 36 others** (2017) How accurate are estimates of glacier ice thickness? Results from ITMIX, the ice thickness models intercomparison eXperiment. *The Cryosphere* **11**(2), 949–970.
- Farinotti D and 6 others** (2019) A consensus estimate for the ice thickness distribution of all glaciers on Earth. *Nature Geoscience* **12**, 168–173. doi: <https://doi.org/10.1038/s41561-019-0300-3>.
- Foster LA, Brock BW, Cutler MEJ and Diotri F** (2012) A physically based method for estimating supraglacial debris thickness from thermal band remote-sensing data. *Journal of Glaciology* **58**(210), 677–691.
- Frolov AD and Macheret YY** (1999) On dielectric properties of dry and wet snow. *Hydrological Processes* **13**(12–13), 1755–1760.
- Gades AM, Conway H, Nereson N, Nozumo N and Kadota T** (2000). Radio echo-sounding through supraglacial debris on Lirung and Khumbu Glaciers, Nepal Himalayas. *Debris-Covered Glaciers*, Washington, USA, International Association of Hydrological Sciences 264, pp. 13–22.
- GlaThiDa Consortium** (2019) Glacier Thickness Database 3.0.1. World Glacier Monitoring Service. Zurich, Switzerland.
- Graham W and McRobie A** (2017) Dipole radar report. Unpublished, see supplementary material.
- Grima C, Blankenship DD, Young DA and Schroeder DM** (2014) Surface slope control on firn density at Thwaites Glacier, West Antarctica: results from airborne radar sounding. *Geophysical Research Letters* **41**(19), 6787–6794.
- Gulley J and Benn D** (2007) Structural control of englacial drainage systems in Himalayan debris-covered glaciers. *Journal of Glaciology* **53**(182), 399–412. doi: [10.3189/002214307783258378](https://doi.org/10.3189/002214307783258378).
- Hindmarsh RCA and 5 others** (2011) Flow at ice-divide triple junctions: 2. Three-dimensional views of isochrone architecture from ice-penetrating radar surveys. *Journal of Geophysical Research: Earth Surface* **116**(F2), F02024, 14, pp.
- IPCC** (2019) IPCC Special Report on the Ocean and Cryosphere in a Changing Climate. H.-O. Pörtner, D.C. Roberts, V. Masson-Delmotte et al.
- Kennett M, Laumann T and Lund C** (1993) Helicopter-borne radio-echo sounding of Svartisen, Norway. *Annals of Glaciology* **17**, 4.
- King EC** (2011) Ice stream or not? Radio-echo sounding of Carlson Inlet, West Antarctica. *The Cryosphere* **5**(4), 907–916.
- King EC** (2020) The precision of radar-derived subglacial bed topography, a case study from Pine Island Glacier, Antarctica. *Annals of Glaciology*, 1–8. doi: <https://doi.org/10.1017/aog.2020.33>.
- King E, Hindmarsh R, Corr H and Bingham RG** (2008) DELORES mark I: construction and operation of the British Antarctic Survey DEep Look Radio Echo Sounder. *International Symposium on Radioglaciology*, Madrid, Spain, International Glaciological Society.
- King O, Quincey DJ, Carrivick JL and Rowan AV** (2017) Spatial variability in mass loss of glaciers in the Everest region, central Himalayas, between 2000 and 2015. *The Cryosphere* **11**(1), 407–426.
- Lambrecht A, Mayer C, Aizen V, Floricioiu D and Surazakov A** (2014) The evolution of Fedchenko glacier in the Pamir, Tajikistan, during the past eight decades. *Journal of Glaciology* **60**(220), 233–244.
- Langhammer L and 6 others** (2019b) Glacier bed surveying with helicopter-borne dual-polarization ground-penetrating radar. *Journal of Glaciology* **65** (249), 123–135.
- Langhammer L, Grab M, Bauder A and Maurer H** (2019a) Glacier thickness estimations of alpine glaciers using data and modeling constraints. *The Cryosphere* **13**(8), 2189–2202.
- Macheret YY, Moskalevsky MY and Vasilenko EV** (1993) Velocity of radio waves in glaciers as an indicator of their hydrothermal state, structure and regime. *Journal of Glaciology* **39**(132), 373–384.
- McCarthy M, Pritchard H, Willis IAN and King E** (2017) Ground-penetrating radar measurements of debris thickness on Lirung Glacier, Nepal. *Journal of Glaciology* **63**(239), 543–555.
- Miles KE and 6 others** (2018) Polythermal structure of a Himalayan debris-covered glacier revealed by borehole thermometry. *Scientific Reports* **8**(1), 16825.
- Nicholson LI, McCarthy M, Pritchard HD and Willis I** (2018) Supraglacial debris thickness variability: impact on ablation and relation to terrain properties. *The Cryosphere* **12**(12), 3719–3734.
- Nobes DC, Leary SF, Hochstein MP and Henry SA** (1994) Ground-penetrating Radar Profiles of Rubble-covered Temperate Glaciers: Results From the

- Tasman And Mueller Glaciers of the Southern Alps of New Zealand. 1994 SEG Annual Meeting. Los Angeles, California, Society of Exploration Geophysicists: 4.
- Page DF and Ramseier RO** (1975) Application of radar techniques to ice and snow studies. *Journal of Glaciology* **15**(73), 21.
- Pritchard HD** (2019) Asia's shrinking glaciers protect large populations from drought stress. *Nature* **569**(7758), 649–654.
- Randolph Glacier Consortium** (2017) Randolph Glacier Inventory – A Dataset of Global Glacier Outlines: Version 6.0: Technical Report. Colorado, USA, Global Land Ice Measurements from Space.
- Reynolds JM** (1997) *An Introduction to Applied and Environmental Geophysics*. Chichester: John Wiley and Sons Ltd.
- Rignot E, Mouginot J, Larsen CE, Gim Y and Kirchner D** (2013) Low-frequency radar sounding of temperate ice masses in Southern Alaska. *Geophysical Research Letters* **40**(20), 5399–5405.
- Rutishauser A, Maurer H and Bauder A** (2016) Helicopter-borne ground-penetrating radar investigations on temperate alpine glaciers: a comparison of different systems and their abilities for bedrock mapping. *Geophysics* **81**, WA119–WA129.
- Schroeder D and 9 others** (2020) Five decades of radioglaciology. *Annals of Glaciology*, 1–13. doi: [10.1017/aog.2020.11](https://doi.org/10.1017/aog.2020.11).
- Swithinbank C** (1969) Airborne radio Echo sounding by the British Antarctic Survey. *The Geographical Journal* **135**(4), 551–553.
- Wightman WE, Jalinoos F, Sirles P and Hanna K** (2003) *Application of Geophysical Methods to Highway Related Problems*. Lakewood, CO: Federal Highway Administration, Central Federal Lands Highway Division.
- Zamora R and 8 others** (2009) Airborne radar sounder for temperate ice: initial results from Patagonia. *Journal of Glaciology* **55**(191), 507–512.